RSC Mechanochemistry

ROYAL SOCIETY OF CHEMISTRY

PAPER

View Article Online
View Journal

Cite this: DOI: 10.1039/d6mr00014b

Mechanosynthesis of cocrystals and coamorphous binary drug–drug systems with apremilast core: structural and biological studies†

K. Trzeciak,[a] R. Dolot,[a] M. K. Dudek,[a] E. Wielgus,[a] S. Kazmierski,[a] P. Paluch,[a] J. Czernek,[b] J. Brus,[b] K. Wiktorska,[c] I. Wadas,[c] K. Głowacka,[cd] A. Lange[c] and M. J. Potrzebowski *[a]

In this paper, we discuss an issue important for understanding the mechanism of forming pharmaceutical binary systems and their safety in specific therapies. The main aim of this article is to answer the question of whether, in mechanochemical processes, the crystallographic form of the starting substances (substrates) affects the course of the reaction and the nature of the products obtained. Two crystallographic forms of the apremilast (APR), which is a drug used in the treatment of psoriasis and psoriatic arthritis, were utilized. As co-formers, medicines from the nonsteroidal anti-inflammatory drug (NSAID) group were used, including salicylic acid (SA), ethenzamide (ET), and paracetamol (PA) which is classified as an analgesic antipyretic drug (AAD). Each of them has a well-defined crystal structure determined by X-ray diffraction. During the course of the studies, it was found that ball milling of the physical mixture produces cocrystals of APR:SA and APR:ET, whereas APR:PA does not. The difference in reactivity is discussed in the context of the preorganization mechanism and the propensity to disrupt the dimeric structure present in the crystal lattice. The disruption of dimers in the ball mill allows the formation of isolated molecules (SA, ET), which complement the cocrystal structure by positioning themselves in the aromatic pocket of APR. Such a process is not observed in the case of PA. For testing the biological properties of new products, we selected the APR:ET cocrystal as a representative sample. Importantly, biological studies showed that the resulting binary system is cytotoxically safe and does not exhibit any undesirable effects.

Received 28th January 2026
Accepted 25th March 2026

DOI: 10.1039/d6mr00014b

rsc.li/RSCMechanochem

Introduction

APR, a phosphodiesterase-4 inhibitor, is an effective oral medication used in the treatment of psoriasis (PsO) and psoriatic arthritis (PsA).[1–3] PsO and PsA constitute a serious health problem worldwide, carrying significant physical, psychological, and socio-economic consequences.[4–6] According to a WHO report, psoriasis is a common disease, affecting approximately 2–3% of the global population.[7] This means that over 60 million people worldwide live with psoriasis. PsA represents a significant subgroup: around 30% of people with psoriasis also suffer from PsA. This indicates that an estimated 20 million people worldwide have PsA. The disease occurs in every country and affects all races and sexes; however, more cases are noted in Western countries, and fewer in Asian and African populations. APR was approved by the U.S. Food and Drug Administration (FDA) in 2014 for the treatment of adults with active psoriatic arthritis and moderate to severe plaque psoriasis, and in 2019 it was also approved for the treatment of oral ulcers associated with Behçet's disease.[8,9]

The APR as many other drugs is characterized by low aqueous solubility and according to Biopharmaceutics Classification System (BCS) belongs to class II or IV.[10] This inherently limits their oral bioavailability, often necessitating high doses and leading to side effects and variable therapeutic outcomes. The insolubility of active substances is a key challenge in pharmaceutical sciences, as a drug must be dissolved in order to be absorbed by the body. Poor solubility often leads to low and variable bioavailability. There are several approaches that allow overcoming this problem and increasing the solubility of active pharmaceutical ingredients (API).[11,12] These methods can generally be divided into three categories: physical modifications (particle size, crystalline form), chemical modifications (molecular alteration), and formulation-based strategies (use of

[a]Centre of Molecular and Macromolecular Studies, Polish Academy of Sciences, Sienkiewicza 112, 90-363 Łódź, Poland. E-mail: marek.potrzebowski@cbmm.lodz.pl
[b]Institute of Macromolecular Chemistry, Czech Academy of Sciences, Heyrovského nám. 1888/2, Prague 6, Czech Republic
[c]Institute of Biology Warsaw, University of Life Sciences-SGGW, Nowoursynowska 159, 02-787 Warsaw, Poland
[d]Department of Chemistry, University of Warsaw, Pasteura 1, 02-093 Warszawa, Poland

† Dedicated to Professor Frederic Lamaty on the occasion of his 60th birthday.

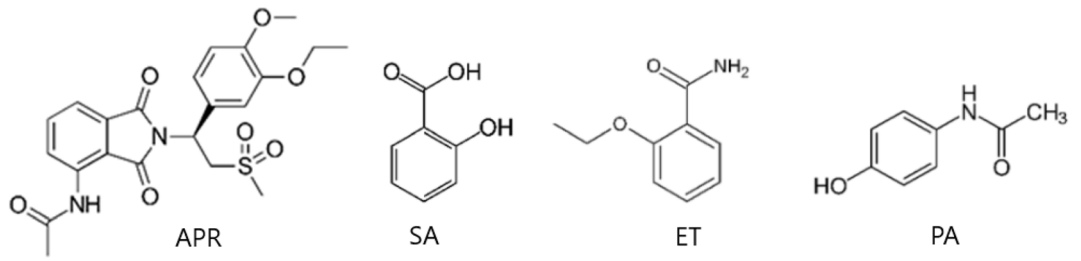

Scheme 1 Chemical structure of APR and the coformers used to prepare the binary systems.

carriers/solvents/coformers). The formation of pharmaceutical cocrystals lies on the boundary between the first and third categories.

Thanks to advances in crystal engineering, a rational approach to modulating properties through the design of pharmaceutical cocrystals has become an effective methodology today.[13] By incorporating a pharmaceutically acceptable coformer into the crystal lattice, cocrystals can form new solid forms with tailored properties.[14–16] This strategy is particularly valuable for APIs such as APR, where the chemical structure cannot be modified. The main goal is to increase kinetic solubility and dissolution rate, thereby improving bioavailability.

The literature describing the formation and physicochemical properties of APR cocrystals is extensive, and many examples have been published over the past decade.[17] Mei and colleagues reported the synthesis of three isostructural APR cocrystals with nicotinamide, caffeine, and acetylsalicylic acid as coformers.[18] It has been demonstrated that the solubility and intrinsic dissolution rate of APR in pH 2.0 buffer are improved through cocrystal formation. Naumkina *et al.* have investigated the cocrystallization of APR with four phenolic-type coformers: phenol, catechol, pyrogallol, and hydroxyquinol.[19] The novel cocrystal forms were characterized using X-ray diffraction and thermal analysis techniques. Dudek *et al.* demonstrated that coformer molecules of an aromatic nature can form cocrystals with APR, where the coformer molecules are located in adjacent APR pockets, forming a sandwich structure with a 1 : 0.5 stoichiometry (API : coformer).[20] To explain the strong preference for forming aromatic interactions in isostructural APR crystals, Dudek *et al.* investigated the features of this special sandwich structure, including the favourable system energy and the stabilizing role of the coformer.[21] π-philic molecular recognition of the APR cavity structure was revealed.

Significant contribution for understanding the strategy for APR cocrystals of preparation comes from the Jirat laboratory.[22] Traditional cocrystal synthesis relies on solution-based crystallization, which is often hampered by solubility mismatches between components, high solvent consumption, and lengthy processes.[23] In contrast, mechanochemical methods, specifically liquid-assisted grinding (LAG), have gained prominence as a green, efficient, and rapid synthetic pathway.[24–30] Liquid assistant (LA) facilitates cocrystal formation through mechanical energy, often achieving quantitative yields after several minutes and minimizing solvent-related issues.[31] It is therefore not surprising that most of the obtained binary APR systems were synthesized using a mechanochemical approach.

In the current work, we present the mechanosynthesis and structural studies of binary systems consisting of APR as the primary component and coformers belonging to NSAIDs: salicylic acid, ethenzamide, and paracetamol, which is classified as an analgesic and antipyretic drug (AAD) (Scheme 1). The motivation for designing these drug–drug cocrystals is the assumption that such a system would enhance therapeutic efficacy through a synergy mechanism. This issue was recently discussed by Grabowski *et al.*[32]

Equally important for our project is the answer to the question of whether, in mechanochemical processes in which a solid material is transformed into new compounds, the crystallographic form of the starting substances (*i.e.* pure or solvate-forms of substrates) affects the course of the reaction and the nature of the products obtained.

Materials and methods

(i) Materials

Ethenzamide, salicylic acid, and paracetamol were purchased from Sigma-Aldrich, while apremilast was obtained from Accel Pharmtech. All compounds were used without further purification.

(ii) Mechanochemical preparation of binary system and form E of APR

The physical mixtures of APR (115 mg) with SA (17 mg), ET (21 mg), or PA (19 mg) in a 1 : 0.5 molar ratio were ground separately with 20 μL of distilled water (for $\eta = 0.15$ μL mg^{-1}) using an MM200 mill. Milling was performed in 10 mL steel jars containing one steel ball ($\varnothing = 10$ mm) for 1 h at an oscillation frequency of 25 Hz. The η parameter was determined as the ratio of the solvent volume (μL) to the sample weight (mg).

Form E of APR was prepared by milling APR (174 mg) with 80 μL of acetonitrile ($\eta = 0.46$ μL mg^{-1}) under identical milling conditions, using an MM200 mill with 10 mL steel jars and one steel ball ($\varnothing = 10$ mm) for 1 h at an oscillation frequency of 25 Hz.

The APR(E):PA sample was prepared by mechanochemical grinding of APR(E) (125 mg) and PA (19 mg) in a 1 : 0.5 molar ratio using an MM200 mill. Milling was conducted in a 10 mL steel jar containing one steel ball ($\varnothing = 10$ mm) for 1 h at an

oscillation frequency of 25 Hz, with external heating applied at 160 °C.

(iii) Differential scanning calorimetry (DSC)

Calorimetric measurements were carried out using a DSC3 instrument (Mettler Toledo, Switzerland) under a nitrogen atmosphere at a heating rate of 10 °C min^{-1}. The APR:SA, APR:ET, and APR:PA binary systems, pure APR, SA, ET, and PA, and their physical mixtures prepared at a 1 : 0.5 molar ratio, were heated from room temperature to 250 °C.

(iv) Solid state NMR measurements

^{13}C CP MAS spectra were recorded on a BRUKER Avance III spectrometer, operating at 400.13 for ^{1}H and 100.03 MHz for ^{13}C, equipped with a MAS probe head using 4 mm ZrO_2 rotors. Spectra were recorded with a MAS frequency of 8 kHz and a proton $\pi/2$ pulse of 4 μs in length and a contact time of 2 ms. The repetition delay (D_1) was 4 s, and the spectral width was 60.0 kHz. Depending on the sample, the FIDs were accumulated with 512 to 1024 scans and time domain size of 2k data points with SPINAL16 decoupling sequence during the acquisition time. A sample of native glycine (α-form) was used for setting the Hartmann–Hahn condition and as an external chemical shift reference (δ(C═O) = 176.50 ppm). Samples were placed in 4 mm zirconia rotors and spun with spinning rate in range 6–8 kHz under the magic angle. The $\pi/2$ pulse was equal to 4.0 μs. SPINAL16 decoupling sequence was employed during the acquisition time. The temperature of samples was controlled employing Bruker Temperature Unit. The 128 transients were coadded with a recycle delay 4 s and an acquired time domain (TD) 4k. Spectral width (SW) was 200 ppm. One-dimensional ^{1}H spectra were recorded on a BRUKER Avance III spectrometer operating at 600.13 MHz for proton nucleus. Samples were placed in 1.3 mm zirconia rotors and spun with spinning rate in range 50 kHz under the magic angle. The $\pi/2H$ pulse was equal to 2.5 μs. The temperature of samples was controlled employing Bruker Temperature Unit. The 16 transients were coadded with a recycle delay 4 s and an acquired time domain (TD) 4k. A spectral width (SW) was 16 ppm. All spectra were recorded and processed with a BrukerTopSpin3.1 program.

(v) Powder X-ray diffraction

The powder X-ray diffractograms were registered with a Panalytical Empyrean diffractometer in Bragg–Brentano horizontal reflection mode, using copper radiation ($\lambda = 1.5418$ Å) and zero-background silicon sample holders. The incident beam path was equipped with a 1/16 diffraction slit, 1/4° anti-scatter slit and 10 mm mask, while the diffracted beam path was equipped with a 7.5 mm anti-scatter slit, and the diffractograms were acquired in 5–40° 2θ range, using a step size of 0.007°.

(vi) Single crystal X-ray diffraction

The single-crystal diffraction measurements were performed using a Rigaku XtaLAB Synergy-S diffractometer equipped with a Cu-Kα radiation source (λ = 1.5418 Å) and a HyPix-6000HE hybrid photon counting detector. Suitable APR:ET crystal was selected, transferred to mineral oil, and mounted on cryo-loops. The crystal was then flash-cooled directly in a N_2 stream. The total number of runs and images was determined based on the strategy calculations performed using the CrysAlisPro by Rigaku (ver. 1.171.42.96a, 2023 and 1.171.43.122a, 2024). The molecular models of the structures were generated with the SHELXT structure solution program by applying intrinsic phasing,[33] and using Olex2 as the graphical interface.[34] The least-squares refinement was carried out with the help of the SHELXL ver. 2018/3 program. All nonhydrogen atoms were refined anisotropically. The proton positions were determined geometrically and refined by using the riding model. The structures were finally validated with CheckCif (https://checkcif.iucr.org) and deposited at the Cambridge Crystallographic Data Centre (CCDC) under the accession number 2513155.

(vii) Dissolution studies

Equilibrium solubility was determined by suspending an excess amount of each sample in 1 mL of simulated gastric fluid without pepsin (SGFsp, pH 1.2) or simulated intestinal fluid without enzymes (SIF, pH 6.8) or Milli-Q water (pH 5.7). The suspensions were equilibrated at room temperature (22 ± 1 °C) for 24 h. After equilibration, the samples were filtered through 0.45 μm PTFE syringe filters, and the filtrates were appropriately diluted with water to obtain concentrations within the linear range of the UPLC–PDA calibration curves.

In vitro dissolution studies were performed using the USP Apparatus II (paddle method) on a dissolution tester (Vision G2 Classic 6, Hanson). An accurately weighed amount of each sample was placed in 1000 mL of Milli-Q water (pH 5.7). The amount of sample and the dissolution medium volume were selected to ensure sink conditions throughout the experiment, with the concentration of dissolved compounds not exceeding 10% of their equilibrium solubility. The temperature of the dissolution medium was maintained at 37 ± 0.5 °C, and the paddle rotation speed was set at 75 rpm. Aliquots of 1 mL were withdrawn at predetermined time intervals (1, 5, 10, 20, 30, 45, and 60 min) and immediately replaced with an equal volume of fresh medium maintained at the same temperature. The collected samples were filtered through 0.45 μm PTFE syringe filters prior to analysis.

The concentrations of the dissolved compounds (APR and coformers) were quantified using an ACQUITY UPLC I-Class system equipped with a photodiode array (PDA) detector (Waters Corp., Milford, MA, USA). Chromatographic separation was achieved on an ACQUITY UPLC™ BEH C18 column (100 × 2.1 mm, 1.7 μm). The detection wavelengths were set at 345 nm for APR, 245 nm for SA, and 235 nm for PAR and ET, based on their respective maximum absorbance values. The mobile phase consisted of solvent A (0.1% formic acid in water) and solvent B (acetonitrile). The flow rate was 0.40 mL min^{-1}, the column temperature was 40 °C and the injection volume was 2 μL. A gradient elution program was applied as follows: 15% B (0–1.0 min), 15–95% B (1.0–4.0 min), 95% B (4.0–4.5 min), 95–15% B (4.5–4.6 min), and 15% B (4.6–7.0 min).

Stock standard solutions of all analyzed compounds were prepared in acetonitrile at a concentration of approximately 10 mg mL^{-1} and stored at 4 °C. These solutions were serially diluted with acetonitrile–water (50 : 50, v/v) to obtain working standard solutions at various concentration levels. Calibration curves were constructed at six concentration points over the range of 1–250 μg mL^{-1} for each compound, with correlation coefficients (R^2) above 0.998. The system was controlled by using the MassLynx software (Version 4.1), and data processing (peak area integration, construction of the calibration curve) was performed by the TargetLynx™ program.

(viii) Theoretical studies

The lattice energies of the considered crystal structures were calculated using CASTEP19.11 code,[35] with PBE functional,[36] employing MDB* dispersion-correction scheme,[37] the cut-off value of 1000 eV and a *k*-point separation of 0.07 A^{-1}, selected on the basis of the convergence tests. Such a choice of the theory level was dictated by a compromise between the computational accuracy and the demand for resources. Recent benchmark conducted for polymorphs of organic crystals has shown that usually such theory level is enough to indicate the correct sign (see Fig. 2.1 in SI of ref. 38), when comparing the energies of two different polymorphs, but to have more reliable values the inclusion of the entropic term (phonon calculations) is necessary. For the purpose of this work such calculations were deemed unfeasible. The experimental crystal structure of APR:ET and the remaining crystal structures extracted from the CSD crystallographic database were first geometry optimized in respect to the atomic positions at the specified level of theory. The crystal structures of APR cocrystals were first reduced to the space group $P4_1$, and for each of these structures, the geometry of the coformer was optimized separately. After the optimization each single component was extracted from the crystal and placed in a cubic box with a 30 Å × 30 Å × 30 Å size to calculate single point energies and hence to get the intramolecular energy contributions. The lattice energy was calculated according to the equation:

$$E_{\mathrm{latt}} = \frac{E_{\mathrm{total}}}{N} - \sum_i E^i_{\mathrm{intra}}$$

where E_{total} is the total energy obtained after geometry optimization, N is the number of symmetry operations in a given space group times the Z' number (for $Z' > 1$ structures), and E_{intra} is the intramolecular energy contribution obtained for isolated molecules.

The stabilization energy of cocrystals was calculated according to the equation:

$$E_{\mathrm{stab}} = \frac{E_{\mathrm{cocr}}}{N} - \sum_i \frac{E^i_{\mathrm{pure}}}{M^i}$$

where E_{cocr} is the total energy of a cocrystal, N and M^i are the number of symmetry operations in a given space group times the Z' number (for $Z' > 1$ structures), and E_{pure} is the total energy of the crystal structures of starting materials.

The molecular electrostatic potential maps were calculated for the CASTEP-optimized isolated molecules, using the Spartan20 software, at the B3LYP/6-311G(d,p) level of theory,[39] and the electron density isovalue of 0.002 e au^{-3}.

(ix) Modelling of the NMR chemical shifts

The periodic density functional theory (DFT) based calculations were carried using the CASTEP code version 16.1.[35,40,41] The crystal structure optimizations and predictions of the NMR chemical shielding were performed in the same way as in the most recent study.[42] The NMR chemical shielding of nuclei in pertinent molecular clusters (see the SI for details) was predicted by the GIAO-B3LYP/6-311++G(2d,2p) approach as implemented in the Gaussian 09 package.[43] This approach was chosen on the basis of its ability to reliably capture an influence of secondary structural effects upon the NMR chemical shifts.[44]

(x) Biological studies

Experimental details describing (a) preparation of compound solutions, (b) mammalian cell and bacterial strains culture (c) mammalian cell viability assay, (d) minimal inhibitory and bactericidal concentration, (d) minimal inhibitory and bactericidal concentration, (e) bacteria viability assay and (f) statistical analysis are attached as SI.

Results and discussion

(i) Mechanosynthesis, solid state NMR, powder X-ray diffraction, and thermal analysis

APR belongs to a group of active pharmaceutical substances that readily form polymorphs and solvates. More than five polymorphic structures of APR have been reported in patents.[45] Form B (according to commonly accepted notation), being the thermodynamically stable polymorph, is used in the formulation of commercial drugs. Several solvates have been described in the literature, including toluene, chlorobenzene, and anisole.[17,20] X-ray data indicate that the solvates form a 'sandwich'-type structure with a stoichiometry of 1 : 0.5. Recently, Zhang *et al.* published the X-ray structure of a new form, called form E, containing acetonitrile molecules in the crystal lattice with a 'sandwich'-type structure in a 1 : 1 ratio (APR : ACN).[46] This form differs from the stoichiometric amount of isostructural solvates containing aromatic solvents. Form E also has different thermal properties and structural features compared to the thermodynamically stable form B (Fig. 1).

The most important difference concerns the size of the 'aromatic pockets.' In the case of form B, which crystallizes in the monoclinic system with the space group $P2_1$ ($Z' = 4$) APR forms two pairs of dimers, the distances between the aromatic planes are 4.23 Å and 4.66 Å. For form E, which crystallizes in the tetragonal system with the space group $P4_12_12$, the distance between the aromatic planes is 7.28 Å. It is worth noting that in all known cocrystal structures, with one exception,[47] the crystal lattice is ordered in the tetragonal system with the space group $P4_12_12$. Therefore, the question of whether form E can be treated as a ready matrix to accommodate a stable coformer in

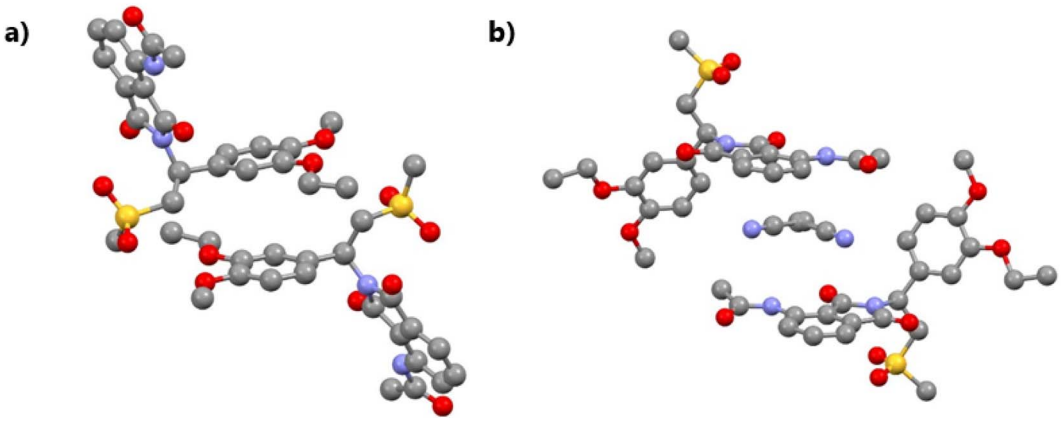

Fig. 1 Crystal structures of APR forms B (a) and E (b). The distances between aromatic planes are *ca.* 4.5 Å in form B and over 7 Å in form E, with acetonitrile molecules acting as a steric barrier.

the exchange process seems entirely justified. Such exchange processes during the mechanochemical transformations are known and for other systems were recently reported.[48,49]

We began our studies with the analysis of a binary system, a physical mixture of APR and SA. We chose such a mixture to test the mechanochemical methodology because, according to literature data APR and SA form cocrystal. Jirat and colleagues, using classical wet cocrystallization, obtained single crystals of a quality suitable for X-ray diffraction studies (CCDC 2049282).[17]

Fig. 2 shows the ^{13}C CP/MAS spectra for the coformers (APR, SA) as well as the obtained APR:SA cocrystal. The spectra were recorded at a spinning rate of 8 kHz at room temperature. In the first approach, polymorph B of APR was used as the substrate for mechanochemical transformations using a ball mill with water as LA. The second component, solid-state SA, occurs as a monoclinic crystal with space group $P2_1/c$, $Z' = 1$, and $Z = 4$ (CCDC refcode SALIAC01). SA molecules in the crystal lattice form hydrogen-bonded dimers with an O···O distance of 2.629 Å (see SI, Fig. S1). The chemical shift of the carboxyl group, at *ca.* 176 ppm reflects the strong character of the hydrogen bond. The hydroxyl group of SA is involved in strong intra-molecular contact (O···O distance 2.593 Å). The chemical shift of C–OH carbon is equal $\delta = 162$ ppm. A comparative analysis of ^{13}C CP/MAS spectra for coformers and the cocrystal shows significant differences. The first and most striking difference is the absence of a signal at $\delta = 176$ ppm. We assume that the carboxyl signal is shifted to the right and overlaps with the APR carboxyl peak. If this assumption is correct, it would indicate that the dimer interaction in SA has been broken, and possibly that in the cocrystal, the isolated molecule is enclosed within an aromatic

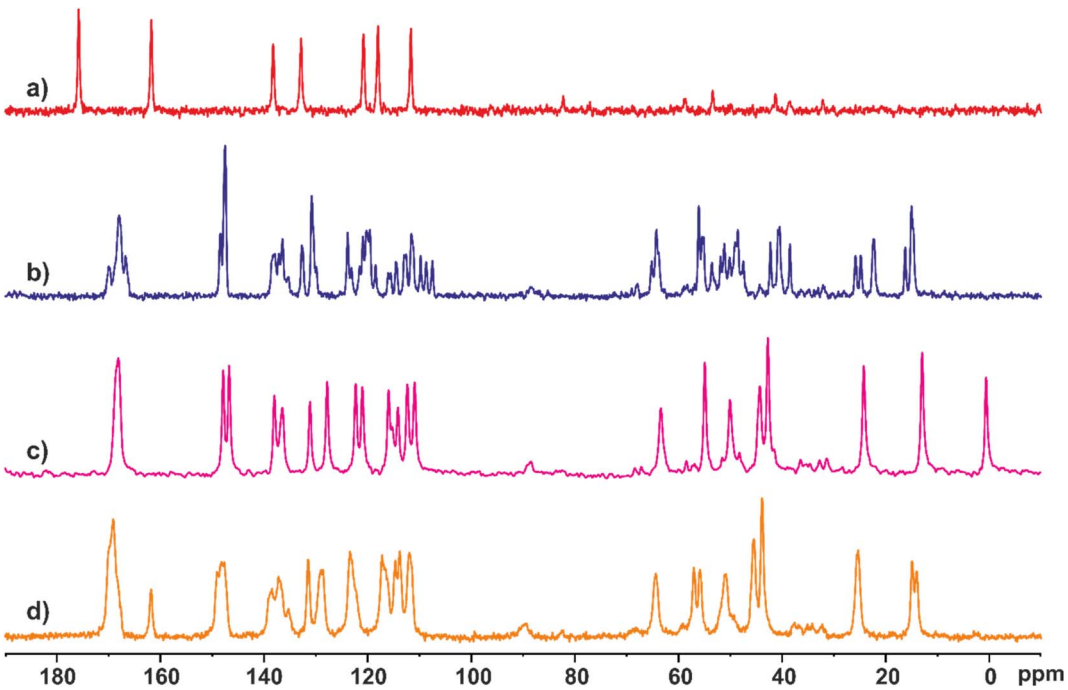

Fig. 2 ^{13}C CP/MAS spectra of (a) SA, (b) APR(B), (c) APR(E), and (d) APR:SA cocrystal recorded with spinning rate 8 kHz at ambient temperature.

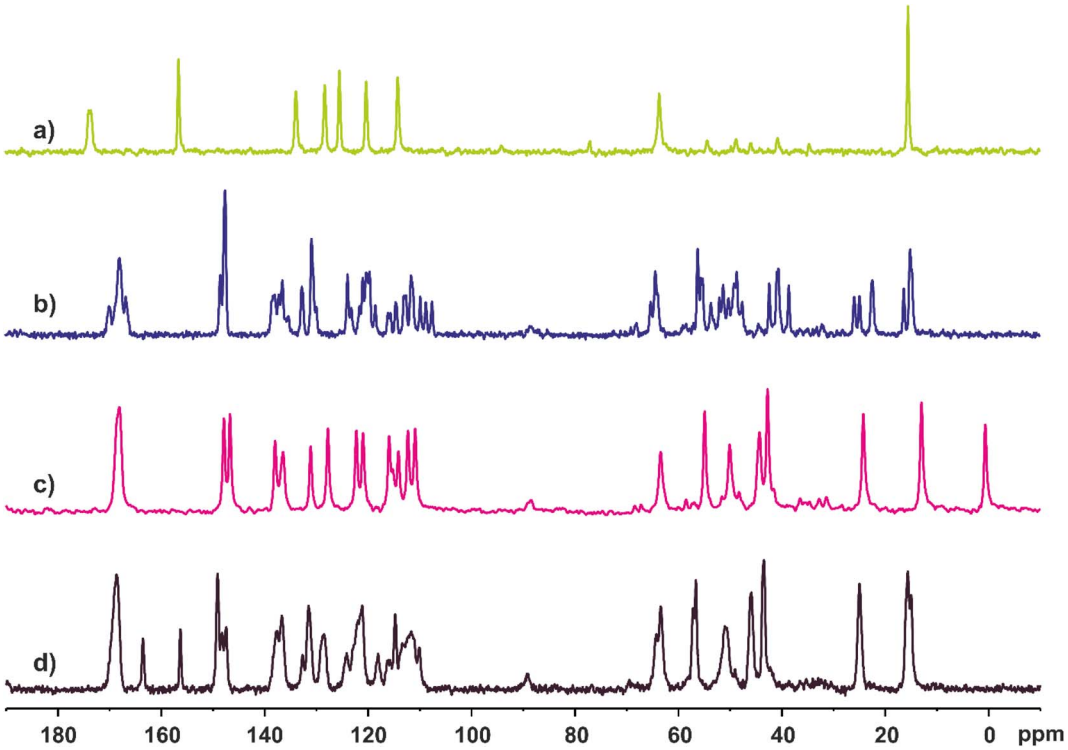

Fig. 3 ^{13}C CP/MAS spectra of (a) ET, (b) APR(B), (c) APR(E), and (d) APR:ET cocrystal recorded with spinning rate 8 kHz at ambient temperature.

pocket. In order to support our hypothesis, changes of relevant peak positions between the SA coformer and in the APR:SA cocrystal were predicted by a combination of the periodic and cluster models using the CASTEP and Gaussian 09 programs, respectively (Materials and methods section). Details of the computational approaches and the key data are provided in the SI (Section 4). It is interesting to note that position of C–OH carbon is unchanged. It means that the strong intramolecular contacts are preserved in SA locked in APR matrix. Further analysis of the spectra also shows differences in the aromatic and aliphatic regions, which can be considered to be an additional evidence confirming the formation of cocrystals. The ^{13}C CP/MAS results are consistent with ^{1}H Very Fast MAS NMR spectra recorded with spinning rate 60 kHz (see SI, Fig. S2).

A clear proof is also provided by the analysis of powder X-ray diffraction (PXRD) data (SI, Fig. S3a). The APR:SA diffractogram confirms that the sample obtained through the mechanochemical process retains high crystallinity. It is worth noting that mechanosynthesis without the presence of water used as a LA does not lead to the formation of cocrystal, but only amorphization of the coformers is observed.

In the next step we have tested mechanochemical synthesis of APR:SA cocrystal employing form E of APR as a starting material. In this case, a high-quality cocrystal was obtained through neat grinding without the addition of a liquid assistant. The claim regarding the absence of LA may be questionable, because in reality, form E is a solvate that contains acetonitrile within the crystal lattice, and the solvent can be considered an internal LA. However, it should not be forgotten that in form E, the size of the aromatic pocket is perfectly suited to accommodate coformer molecules.[50,51] It cannot be ruled out that, in this case, the synergy of both factors facilitates the relatively easy formation of the cocrystal.[17]

Another coformer we used for formation of APR:API cocrystals is ET. According to literature data, ET easily forms cocrystals, and so far many different binary compositions have been reported.[52–56] However, to the best of our knowledge, no attempt has yet been made to obtain an APR:ET cocrystal.

Fig. 3 shows the ^{13}C CP/MAS spectra of coformers and APR:ET cocrystal. Form B of APR was used for synthesis of new binary form. The crystal structure of ET was reported by Pagola and Stephens.[57] ET crystallizes in monoclinic system with $P2_1/n$ space group, $Z' = 1$ and $Z = 4$ (CCDC refcode DUKXAJ). In the crystal lattice the amide substituents are linked into centrosymmetric head-to-head hydrogen-bonded dimers (SI, Fig. S2). The distances between donor and acceptor are 2.917 Å for N1–H1A···O1 and 2.860 Å for N1–H1B···O1, respectively. The chemical shift value of the ^{13}C of the carbonyl residue of the amide group ($\delta = 173$ ppm) is typical for systems involved in the formation of strong hydrogen bonds.

The APR:ET cocrystal was obtained in a ball mill using water as a LA. The contribution of water is crucial for the successful course of the synthesis process. As in case of SA without LA, only amorphization of the coformers is observed. Similar to SA, the shift in the position of the carboxyl/carbonyl group is a simple and sensitive probe that shows whether a cocrystal has been formed or not. Analysis of the APR:ET ^{13}C CP/MAS spectrum revealed a change in the chemical shift value of the C═O group

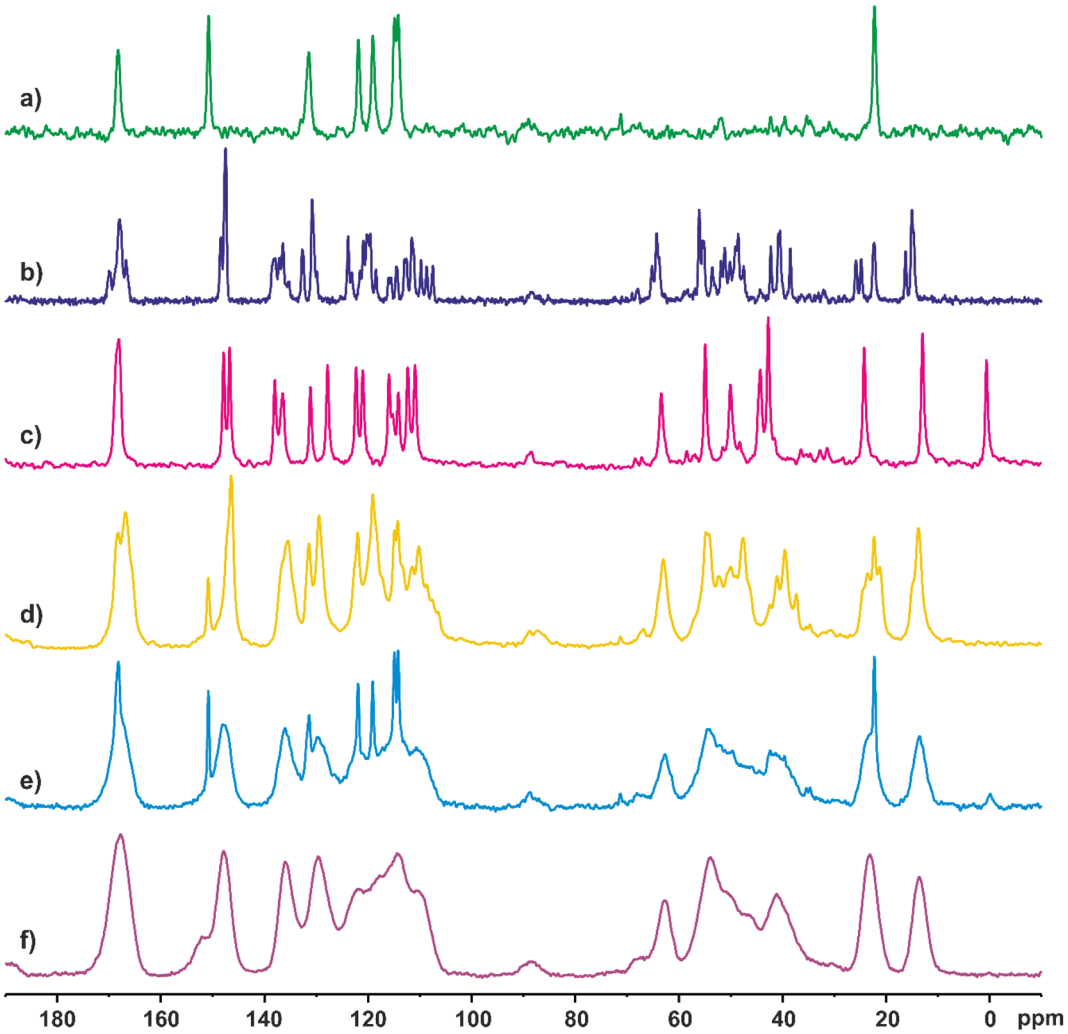

Fig. 4 ^{13}C CP/MAS spectra of (a) PA, (b) APR(B), (c) APR(E), (d) APR(B):PA in 1 : 0.5 molar ratio after grinding with 20 μl of distilled water, (e) APR(E):PA in 1 : 0.5 molar after neat grinding, and (f) APR(E):PA in 1 : 0.5 molar after thermomechanical approach. All spectra were recorded with spinning rate 8 kHz at ambient temperature.

from $\delta = 173$ ppm to $\delta = 165$ ppm. Such a significant difference is very likely related to conformational changes involving the amide group. The correlation between NMR experimental data and computed results is discussed in the SI (Section 6). ^{1}H VF MAS NMR spectra are shown in Fig. S2 (SI).

We assume that during the mechanochemical process, the dimer structure is destroyed, the amide group rotates around the C–C bond, and one of the hydrogen atoms of the NH_2 residue participates in forming an intramolecular hydrogen bond with the neighbouring ethoxy group O–CH_2CH_3. In this way, the ET molecule becomes planar and fits better into the aromatic pocket of APR. The mechanism of this process was discussed in detail in our previous work.[36] As in case of APR:SA cocrystal inspection of the spectral pattern in aromatic and aliphatic region of APR:ET confirm the formation of new well organized binary system. Additional proof provides the analysis of PXRD data (SI, Fig. S3b) for ET, APR (form B) and APR:ET cocrystal. We obtained interesting results when testing form E in the mechanosynthesis of the APR:ET cocrystal. In this case, the cocrystal was obtained using a neat grinding procedure without the addition of LA. If ET is used as coformer the quality of obtained cocrystal is very high.

The most demanding case we encountered during our study on the mechanochemical synthesis of APR cocrystals involves the use of PA as a coformer. PA forms three well defined polymorphs. The crystal structures of two of them, known as form I (monoclinic, space group $P2_1/n$, reference code CCDC HXACAN01) and form II (orthorhombic, space group *Pbca*, reference code CCDC HXACAN23), were described by Druzhbin *et al.*[58] Obtaining form III is more challenging, and several research groups have tested various approaches, mainly thermal methods, which have proven most promising.[59,60] Form III crystallizes as orthorhombic system with space group $Pca2_1$ (CCDC 716555 and 716554). It should be emphasized that for each polymorph, strong hydrogen bonds and specific higher order arrangements stabilize the crystal lattice (see SI, Fig. S1c) The most stable is form I, which is also the commercial form.

Fig. 4 shows the ^{13}C CP/MAS spectra of coformers and the sample obtained through the mechanochemical procedure. Unfortunately, in this case, we do not have such a convenient

NMR probe (diagnostic signals) that would allow us to track the progress of the transformation in the ball mill. The NMR peak of the carbonyl group HN–C(O)–CH_3 of polymorph I (Fig. 4a) is located exactly at the same position as the carboxyl residue of APR (Fig. 4b).

In the case of APR(B), water was used as a LA during mechanochemical synthesis. Analysis of the NMR spectra does not provide a clear answer as to whether a cocrystal is formed. First, the ^{13}C signals of PA, except for the C–OH carbon ($\delta = 152$ ppm), overlap with the APR resonances. Second, the APR signals are very broad, which rather suggests sample amorphicity than the formation of a cocrystal. An attempt to obtain the APR:PA cocrystal by using APR in form E (without LA) and polymorph I of PA was unsuccessful. In this case, we observed amorphization of APR, while PA retained its crystalline form (see Fig. 4d). The sharp NMR lines visible in Fig. 4d and e represent paracetamol in the crystalline state as polymorph I. Ultimately, considering that the form III PA is obtained through a thermal procedure, we decided to test a thermomechanical approach. For the synthesis in a ball mill, we used APR in form E, since the melting temperature of this sample is around 100 °C, which is 60 °C lower compared to APR in form B. The coformer used was polymorph I of PA, which was applied in the hope of inducing the I–III polymorphic transformation in the presence of APR. Fig. 4f shows the ^{13}C CP/MAS spectrum of the sample obtained using the procedure described above. Analysis of the spectrum indicates that the sample is completely amorphous. There are no sharp signals typical for crystalline forms. The NMR results are fully consistent with the PXRD data shown in Fig. S3c (see SI).

The problem with obtaining the APR:PA cocrystal we are trying to rationalize, taking into account the preorganization mechanism leading to the formation of the cocrystal in mechanochemical approach. In two previous successful cases, *e.g.*, APR:SA, APR:ET, during grinding, the dimeric structure of the coformers SA and ET was destroyed (see NMR data), and then the isolated molecule was able to complement the cocrystal structure, positioning itself in the aromatic pocket of APR. We assume that PA polymorphs are more stable compared to SA and ET, and consequently the forces of the crystal lattice prevent the destruction of dimeric and higher-order structures in the ball mill. As a result, one of the prerequisites for successful synthesis, which determines the stoichiometry of the cocrystal (APR:API, 1 : 0.5), cannot be met.

On the other hand, the preparation of amorphous active pharmaceutical ingredients (APIs) is one of the effective strategies in drug formulations, used to increase their solubility and bioavailability. This approach is very often associated with the formation of binary co-amorphic systems, in which the spontaneous phase transition of the API into a crystalline form is delayed and/or the recrystallization process is significantly reduced. Very recently, this second strategy was applied to the formulation of APR. For example, Pardhi *et al.* reported the preparation and physicochemical studies of a drug–drug coamorphous (CAM) system consisting of APR and Indomethacin (INDO), which belongs to the group of nonsteroidal anti-inflammatory drugs (NSAIDs). The authors found that the coamorphous system was stable for five months at a temperature of 40 ± 2 °C and a relative humidity of 75 ± 5%.[61] Patzmann and colleagues, co-milling of fenofibrate (FEN) and APR, tested the effect of low and high glass transition temperatures on the stability, solubility, and dissolution kinetics of the obtained coamorphous compound. Finally, Samanthula and coworkers investigated drug–drug coamorphous systems (CAMs) containing APR and aceclofenac (ACE). Three monophase CAMs systems were prepared consisting of APR and ACE in molar ratios of 1 : 1, 1 : 2, and 2 : 1, using the melt-quenching method.[62] CAM showed significantly better solubility and dissolution over time, while accelerated stability tests lower degradation rates.

Distinguishing between a physical mixture of amorphous components and a co-amorphous system is not trivial. There is no single universal technique that would provide a definitive answer. The SI include an extensive section (SI, Section 4) in which we present the arguments that led us to propose the hypothesis that the studied object is a co-amorphous system. Our conclusions are based on the analysis of solid-state ^{13}C NMR spectra in the context of monitoring the time-controlled transition of paracetamol from the glassy state to the crystalline state, the stability study of the APR:PA sample over a period of three months, measurements of ^{1}H T_1 relaxation times for both samples and the comparative analysis of the glass transition temperature (T_g) of pure amorphous apremilast and amorphous APR:PA. (Fig. S4a–c, S5a, b, and S6). Our experimental results are further supported by the theoretical studies presented in Section (iv).

The ultimate proof confirming the formation of APR:SA and APR:ET cocrystals, as well as the lack of success in the case of the binary APR and PA system, is the thermal analysis of the substrates and products. The appropriate thermograms for each of the discussed cases are attached as supplementary information (see SI, Fig. S7a–c).

(ii) Single crystal X-ray diffraction of APR:ET sample

To grow single crystals, APR and ET in a 1 : 0.5 molar ratio were dissolved in acetonitrile, heated to 80 °C, and left at room temperature to allow slow evaporation until single crystals formed in the vial. Suitable crystals were collected and subjected to single-crystal structure determination, which provided insights into the three-dimensional structure of the cocrystal. To the best of our knowledge, this is the first report of the crystal structure of the APR:ET cocrystal.

The crystallographic data for the APR:ET cocrystal are summarized in Table S1 (see ESI). The obtained APR:ET is isostructural with previously published APR cocrystals or solvates[17–20,22,63,64] This new solid form crystallized in the tetragonal system with the $P4_12_12$ space group and cell parameters $a \approx 13$ Å and $c \approx 29$ Å. The APR to ET ratio was confirmed as 1 : 0.5. The asymmetric unit contained one molecule of APR and half a molecule of ET. A two-fold rotation axis intersects ET, which is disordered with 50% occupancy over two positions, as shown in Fig. 8. As previously observed, APR molecules and the coformer interact through weak

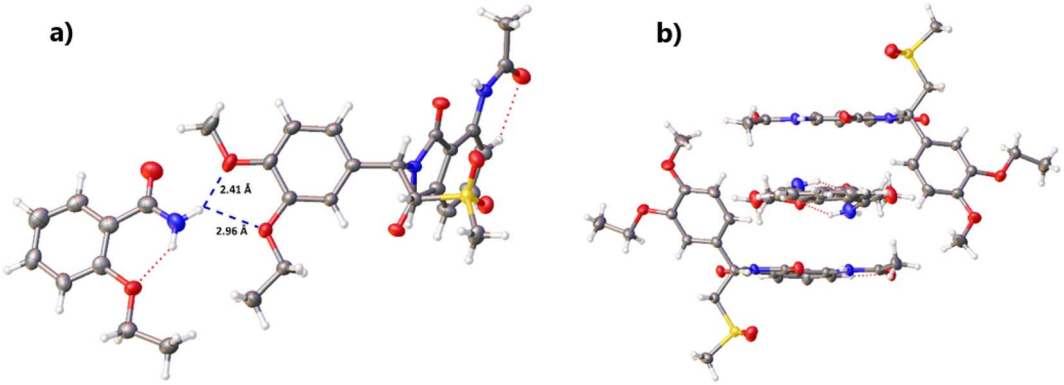

Fig. 5 Crystal structure of APR:ET cocrystal: (a) view of the asymmetric unit; (b) trimolecular motif consisting of two APR molecules and one ET molecule.

intermolecular forces such as hydrogen bonds, π–π interactions, and van der Waals forces. ET and APR molecules are held together by a hydrogen bond formed between the amide group of the coformer and the ethoxy and methoxy groups of the APR molecule (Fig. 5a). The guest molecule is captured in nearly the same position as previously observed, forming a trimolecular motif with the two APR molecules. The phthalimide part of the APR molecules and the benzene ring of the ET are nearly parallel (Fig. 5b).

(iii) Dissolution studies

The main goal of this part of the project is to answer the question of how the formation of cocrystals and coamorphous systems affects the solubility of APIs and the kinetics of their dissolution. For this purpose, several samples were used, starting from the pure APR ingredient in various solid state forms and binary APR systems: APR:SA, APR:ET, and APR:PA. The study began with a solubility analysis, with particular attention to the content of APR in the liquid phase. Measurements were conducted at room temperature (22 ± 1 °C) in simulated gastric fluid without pepsin (SGFsp, pH 1.2), in simulated intestinal fluid without enzymes (SIF, pH 6.8) and Milli-Q water (pH 5.7).

Fig. 6 graphically illustrates significant differences in APR solubility, which depend not only on the composition of the binary system but also on the organization of the solid state of the APR sample. It can be seen that at pH 1.2, the solubility of amorphous APR, obtained by melting[20,40] APR(M), is about 15 times higher compared to the commercial APR(B) sample while solubility of APR(E) is close to APR(M). The solubility of the binary system also differs significantly. The solubility of APR:ET is 60% higher, while that of APR:SA is 50% lower compared to APR(B). The case of APR:PA, which occurs in an amorphous form, is very specific. The solubility of this sample is about 19% higher than APR(M).

At pH 6.8, the solubility of all samples is slightly lower, except for the APR:SA cocrystal, for which the opposite trend is

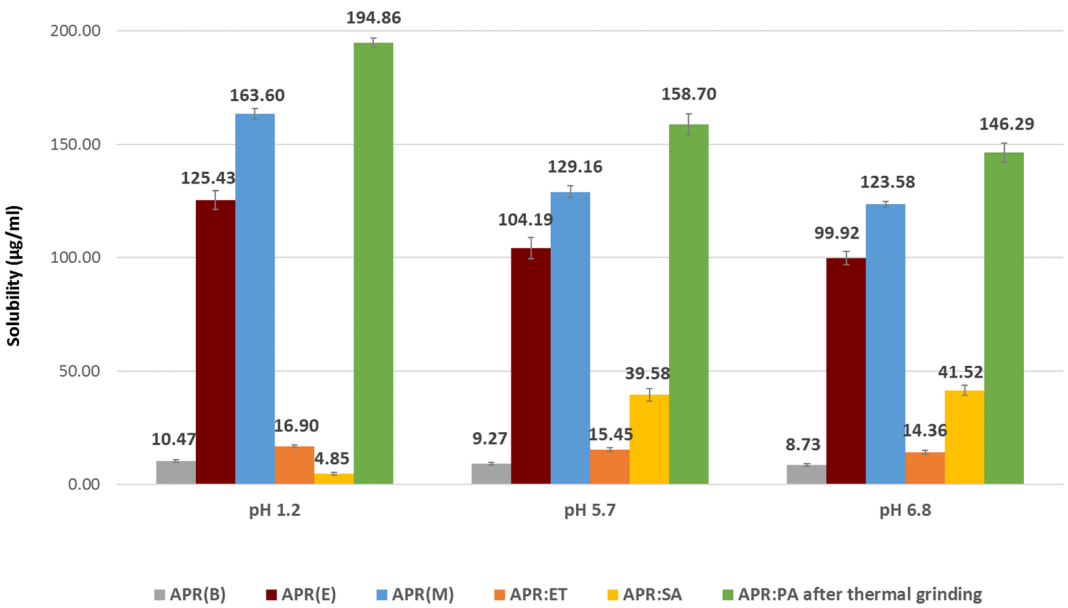

Fig. 6 Equilibrium solubility of APR, its cocrystals (APR:ET and APR:SA), and coamorphous binary system APR and PA in various pH buffers.

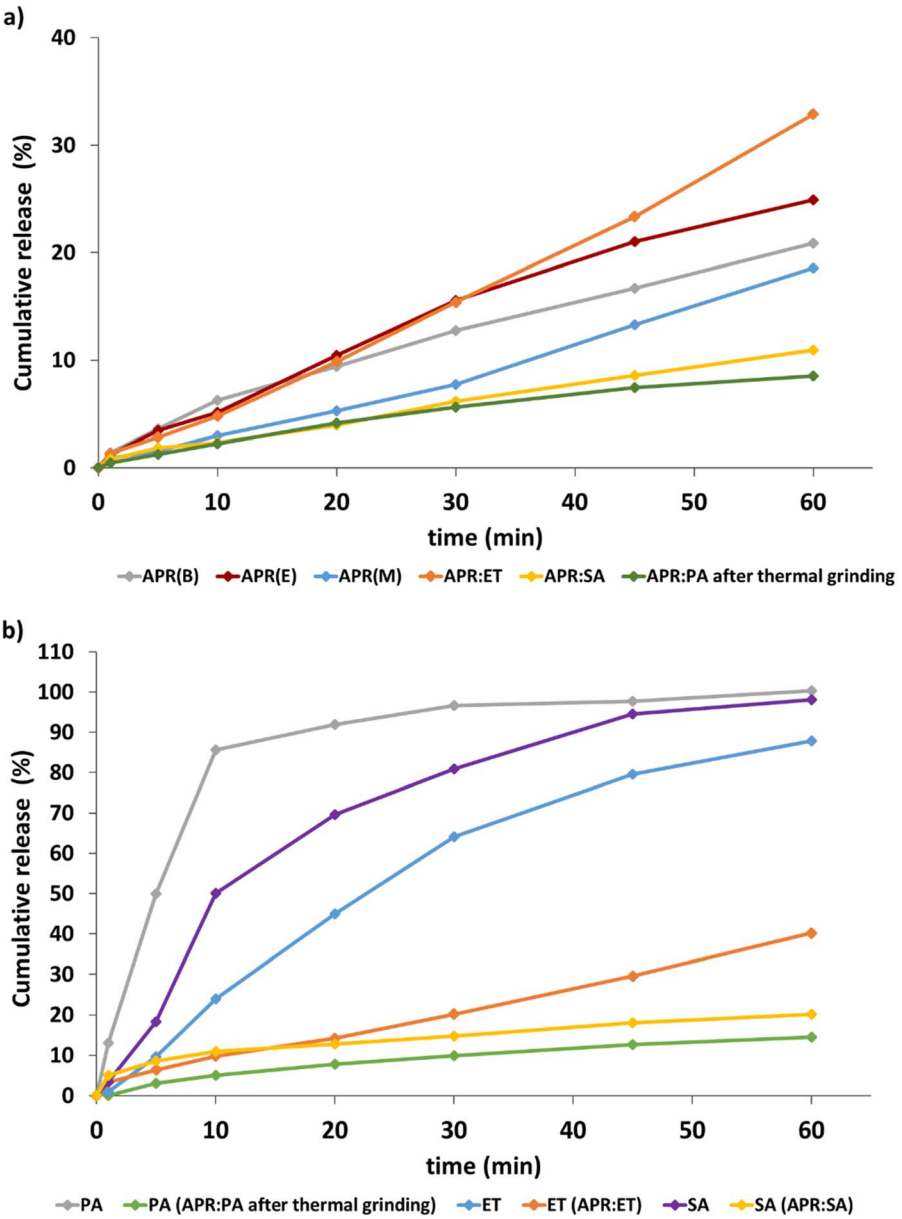

Fig. 7 Dissolution profiles of: (a) various solid state forms of APR, as well as APR in APR:ET, APR: SA, and APR:PA after thermal grinding, (b) pure ET, PA, SA, and ET, PA, SA in APR:ET, APR:SA and APR:PA after thermal grinding, respectively. Water with pH 5.7 was used as a dissolution medium. The estimated error in measurements was found to be +/−1%.

observed. This discrepancy can be explained by the ionization behavior of SA. SA is a weak acid with a pK_a of 2.98. Therefore, at the experimental pH of 6.8, which is significantly higher than its pK_a, the Henderson–Hasselbalch equation predicts that the compound exists almost entirely in its dissociated (ionic) form. Consequently, as the ionized species possesses significantly greater aqueous solubility than the neutral form, the theoretical solubility under these conditions is exceptionally high. This effect can be a driving force leading to an unexpected increase in APR concentration in a solution with a pH of 6.8.

At pH 5.7 (Milli-Q water), the solubility of the studied systems exhibits intermediate behavior between strongly acidic conditions and intestinal-like conditions. The increase in solubility observed for the amorphous form of apremilast APR(M) and APR(E) compared to the commercial APR(B) is still significant. Furthermore, the solubility of all samples at pH 5.7 generally follows the same trend observed at pH 6.8, suggesting that similar physicochemical factors influence the behavior of the studied systems under both conditions.

Fig. 7 shows the dissolution profiles for pure components as well as binary systems analyzed in water at pH 5.7 over a time range from 0 to 60 min. In Fig. 7a, the dissolution kinetics of APR as a function of time are shown. It is quite surprising, in light of the results presented in Fig. 6, that after 60 min, the concentration of APR as part of the cocrystal system APR:ET is the highest (32.88%), higher compared to APR(E) (24.93%), APR(B) (20.89%) and APR(M) (18.58%). The lowest concentration of APR in the liquid phase was observed for the

Table 1 Stabilization energies of the formation of cocrystals/solvates in each row in respect to a parent form given in each column. The values are in kJ mol^{-1}, and for ACN solvate include entropic penalty for going from liquid to the solid state

	APR(B)	APR(E)	APR:SA	APR:ET
APR(B)	0			
APR(E)	−1.24	0		
APR:SA	−8.04	−6.80	0	
APR:ET	−3.57	−5.15	−4.47	0
APR:CIN	4.79	5.58	0.77	12.38

coamorphous sample APR:PA (8.56%) and slightly higher for the cocrystal system APR:SA (10.94%).

Fig. 7b shows the dissolution profiles of the components that complement APR in forming binary systems. As expected, SA, ET, and PA dissolve quickly and reach values close to 100% after 60 min, although it should be noted that the concentration of ET is slightly lower (87.8%). The dissolution kinetics of binary systems studied by monitoring coformer profiles clearly show the same trend as observed in Fig. 7a for APR. After 60 min, the concentration of ET in the liquid phase is the highest, while for PA it is 3.5 times lower.

At the first glance the results presented in Fig. 6 and 7 seems to be confusing. When we compare the water solubility of the coamorphous APR:PA system with the cocrystal APR:ET, after 24 h there is 10 times more apremilast in solution for the coamorphous sample. However, when we examine the release kinetics, after 60 min there is 3 times more apremilast in solution for the cocrystal APR:ET than for the APR:PA. These discrepancies can be explained by considering the fact that thermodynamic control and kinetic control can describe different intermediate stages and different mechanisms. Such differentiation as described above is not surprising in the analysis of binary pharmaceutical systems, and similar cases are described in the literature.[65]

(iv) Explanation of the preferences for forming cocrystals and coamorphs using theoretical calculations

In majority of cases, as shown recently by Taylor and Day,[66] the formation of cocrystals is a thermodynamically driven process, meaning that the cocrystal stabilization energy, E^{stab}, *i.e.* the difference between the total energy of a cocrystal and the sum of the total energies of the crystal forms of substrates, is negative. As a result, the E^{stab} value can often be used as a first indicator of the feasibility of cocrystallization process, provided that the entropy term does not play a significant role in stabilization. In our calculations, we have evaluated the stabilization energies of all of the studied systems in respect to each other. In addition, we included a previously published cocrystal of APR with cinnamic acid (APR:CIN). This was done because APR:CIN is the only known example of non-isostructural cocrystal of APR, Crystallizing in $P2_12_12_1$ space group, instead of $P4_12_12$ space group. Such 'symmetry breaking' was attributed to the size of cinnamic acid molecule, which is similar to the size of PA. Table 1 shows the obtained stabilization energies for the considered crystal forms in respect to the appropriate substrates, calculated for all possible combinations of substrates and products. The E^{stab} are calculated in respect to a crystal given in each column. For each row, negative values of E^{stab} (blue) mean that the formation of a given form in a row should be energetically preferred over the parent form in a column. For example, the values in the first column refer to the stabilization energy in respect to APR form B, and indicate that both drug–drug cocrystals (with SA and ET) should be thermodynamically favoured over the parent forms. This is visible as a negative stabilization energy value of −8.04 kJ mol^{-1} in APR(B) column and APR:SA row, as well as a negative E^{stab} value of −3.57 kJ mol^{-1} in APR(B) column and APR:ET row. In contrast, the E^{stab} for APR:CIN in respect to APR(B) is positive (red) and equal to +4.79 kJ mol^{-1}.

The analysis of Table 1 reveals that the formation of APR cocrystals with SA and ET is enthalpy-driven, regardless of whether APR(B) or APR(E) (solvate) is used as a reference. Indeed, the performed experiments showed that both cocrystals are easily formed in the tested mechanochemical conditions. Surprisingly, the stabilization energies of these forms in respect to APR(E) are, contrary to our expectations, less negative, despite the fact that APR(E), APR:SA and APR:ET are isostructural. It means that the preorganization does not facilitate cocrystal formation from the point of view of solely the energetic criteria. It is also interesting to note, that the energy gain in APR:ET and APR:SA has a different source. Table S4 shows intra- and intermolecular contributions to the E^{stab} for each of the analysed cocrystals. The intramolecular contribution to the E^{stab} for APR:SA is positive and equal to +6.55 kJ mol^{-1}, which is compensated by a significant intermolecular contribution to E^{stab}, equal to −14.59 kJ mol^{-1}. In contrast, for APR:ET the intramolecular and intermolecular contributions are equal, respectively, to −5.96 kJ mol^{-1} and +2.39 kJ mol^{-1}. This change in intramolecular energy in APR:ET is associated mainly with the conformational change of ET, which in the cocrystal can assume its most energetically stable conformation, featuring an intramolecular hydrogen bond between one of the NH_2 protons and its ethoxy oxygen.

Another unexpected result is that of the APR:CIN stabilization energy to be positive in respect to every other evaluated form of APR, which indicates that the formation of this form is not enthalpy-driven. Recent estimates indicate that around 5% of cocrystals fall into this category,[66] including APR cocrystals with picolinamide, imidazole, hydroquinone and resorcinol.[21] This, however, was not anticipated for APR:CIN, since there is

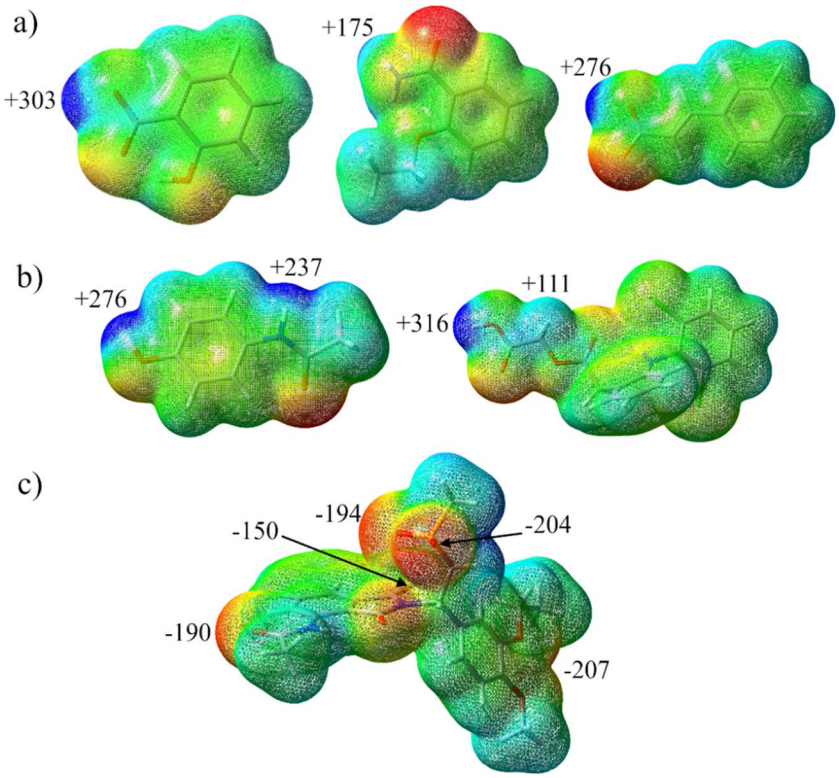

Fig. 8 Molecular electrostatic potential maps mapped onto an electron density isosurface (isovalue 0.002), calculated at the B3LYP/3-611G(d,p) level of theory for (a) compounds forming cocrystals with APR (from left: SA, ET, and CIN), (b) compounds forming co-amorphous mixtures with APR (PA and ACE), and (c) APR. Energies given are in kJ mol^{-1}.

no disorder present in this crystal form, and it was the disorder present in all isostructural APR cocrystals which was postulated to be a driving force for cocrystal formation of the forms with positive stabilization energies.

In the case of PA no cocrystal with APR was obtained, despite significant experimental effort, but the reactions resulted in coamorphous mixtures, especially if temperature was increased. It has been shown that the size of the coformer can be a significant hindrance the APR cocrystal formation, with CIN being the largest one to still form a cocrystal, albeit in a lower symmetry space group.[17] The size, however, does not seem to be an issue with PA, since its longest axis has almost the same length of the longest axis as that of CIN (9.127 Å *vs.* 9.167 Å), and the same goes for molecular volume (158 $Å^3$ *vs.* 160 $Å^3$). Therefore, to investigate the possible reasons for that we investigated the molecular electrostatic potential maps (Fig. 8) calculated for SA, ET, CIN (Fig. 8a), PA (Fig. 8b) and APR (Fig. 8c). Additionally, we included in MEP calculations aceclofenac (ACE) (Fig. 8b), which has been recently found to form a coamorphous mixture with APR.[62]

Fig. 8c shows that APR has only one site with a markedly positive electrostatic potential, already engaged in an intramolecular hydrogen bond (NH···O=C), and multiple sites with a strongly negative electrostatic potential. In the majority of APR cocrystals and solvates these negative sites do not form any directional interactions, with a small exception of coformers capable to form COOH···OEt/OMe interaction with APR, which includes SA and CIN. To form this interaction, both coformers need to have a strongly electron-deficient site, somewhat removed from the vicinity of the aromatic ring to which it is substituted. The rest of the known binary forms of APR are stabilized almost entirely by aromatic–aromatic interactions. This is also the case of APR:ET cocrystal. This coformer, although potentially having two positive interaction sites (two NH_2 hydrogen atoms), forms an intramolecular hydrogen bond in the cocrystal, thus assuming its most energetically favourable conformation. Similarly, SA forms an intramolecular hydrogen bond in the aromatic pocket of its cocrystal with APR. In contrast to that, the molecules that forms coamorphous mixtures (PA and ACE, Fig. 8b) have at least two electron-deficient regions, possibly able to disrupt the favourite aromatic pocket arrangement of APR. They also do not have any capacity to form intramolecular interactions stabilizing their conformations inside the pocket.

(v) Biological studies

To assess the potential cytotoxicity of APR, ET, or their cocrystal, their impact on the set of selected model cells was assessed. The mammalian fibroblast NIH3T3 cells exhibit high sensitivity to the chemical compounds and are commonly used as a model cell line in toxicological studies.[67] The selected microorganisms (*S. aureus*, *S. epidermidis*, *P. aeruginosa*, and *E. coli*) represent clinically relevant Gram-positive and Gram-negative bacterial species associated with the human microbiota and

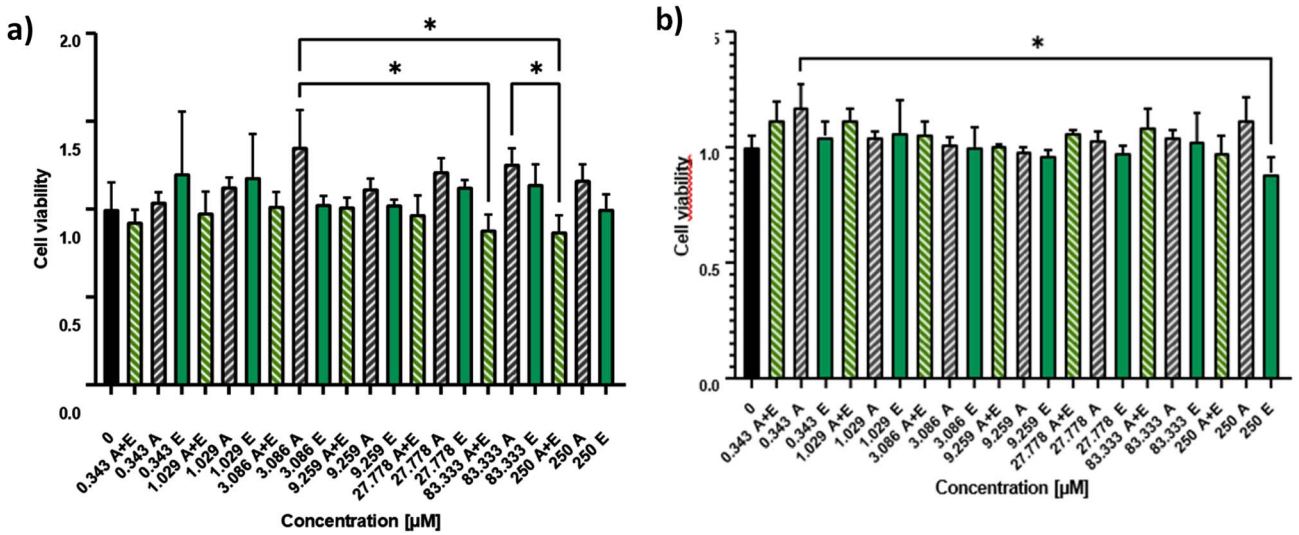

Fig. 9 Effects of different concentrations of compounds on cell viability after (a) 24 and (b) 72 h (MTT assay). Data represent mean ± SD ($n = 4$) and are normalized to control cells incubated only with DMSO (0.1%). Statistically significant differences between pairs of concentration data were assessed using Dunn's test.

opportunistic infections. Since they commonly colonize and inhabit the human skin and mucosal surfaces, their inclusion provides a representative panel for evaluating the interaction and safety profile of the studied new drugs.

The MTT assay on NIH3T3 cell line showed no statistically significant toxicity for APR, ET or APR:ET cocrystal. Statistical analysis revealed statistically significant differences only between different incubation conditions (specifically, varying concentrations and compounds). No statistically significant differences were observed between compounds at the same concentrations, nor between different concentrations of the same compound. Moreover, no statistically significant differences were observed compared to the control (Fig. 9). It is notable that the cocrystal exhibited a slight trend of increased toxicity at 24 h. This may be explained by the occurrence of physical interactions between the cocrystal and the cell membrane at shorter incubation times, whereas after drug release (dissolution) at longer incubation times (72 h), no cytotoxicity was exhibited by the cocrystal form of the drug. Microscopic evaluation after incubation with low (0.343 μM), medium (9.259 μM), and high (250 μM) concentrations confirmed the absence of changes in cell number or morphology, suggesting that any cocrystal-related effects are limited to subtle metabolic alterations rather than cytotoxicity (SI, Fig. S8a and b).

To further evaluate toxicity, minimum inhibitory concentration (MIC) and minimum bactericidal concentration (MBC) assays were conducted. Neither MIC nor MBC values could be determined, as no antimicrobial activity was observed (SI, Table S2, Fig. S8c). All tested bacterial strains continued to grow in the presence of the compounds, which was further confirmed by bacterial viability assays. Microbial viability remained statistically comparable to untreated controls across all concentrations, indicating no interference with bacterial proliferation under the applied experimental conditions.

Conclusions

In this work, we presented a mechanochemical approach to the synthesis of binary drug–drug systems. The main idea of this project was to develop a medicine dedicated to a specific disease, whose therapeutic effect was enhanced with a pain-relieving and anti-inflammatory component. Our studies have clearly shown that even within a group of coformers belonging to the same class of drugs (NSAIDs in this case), different strategies must be employed when grinding the ingredients in a ball mill. When preparing cocrystals using the commercially available polymorph of apremilast known in the literature as form B, the presence of LA was necessary. In the case of the apremilast solvate containing an acetonitrile molecules in the crystal lattice (the polymorph E), grinding without additives yielded the expected products. This effect was particularly evident when SA and ET were used as coformers. In the case of a coformer that does not meet the structural criteria to form cocrystals using the standard mechanochemical procedure, attempts to convert the mixture into the desired product through a thermomechanical approach results in the formation of a coamorphous sample. This situation was observed in the mixture of APR and PA. It is worth noting that when the thermomechanical method is the preferred approach, the APR(E) form represents a reasonable option for further transformations. The melting point of APR(E) is 60 °C lower compared to APR(B); the lower temperature can be used for transformations, which may protect the API from thermal degradation. For biological studies, APR:ET cocrystal was chosen as a representative sample. Cytotoxicity and antibacterial tests showed that the resulting binary system is safe in terms of cytotoxicity, does not exhibit any other undesirable effects, and can be used in therapies.

Conflicts of interest

There are no conflicts to declare.

Data availability

CCDC 2513155 contains the supplementary crystallographic data for this paper.[68]

The supporting data has been provided as part of the supplementary information (SI). Supplementary information: (1) X-ray structure of coformers SA, ET, and PA. (2) ^{1}H very fast MAS NMR. (3) Powder X-ray diffraction data, experimental and calculated diffractograms. (4) Arguments for treating the binary system APR:PA as a coamorphic sample (5) DSC curves for APR(B), APR(E), SA, ET, PA, and binary systems APR:SA, APR:ET, and APR:PA. (6) Experimental data for single crystal X-ray analysis of APR:ET. (7) Modeling of the NMR chemical shifts. (8) Biological studies. (9) Solubility studies. (10) Theoretical calculations. See DOI: https://doi.org/10.1039/d6mr00014b.

Acknowledgements

This work was supported by the Polish National Science Centre (NCN) [Grant No. UMO 2022/47/I/ST4/01629]. The purchase of the Rigaku Oxford Diffraction XtaLAB Synergy-S single-crystal X-Ray diffractometer was supported by the EU Regional Operational Program of the Lodz Region, RPLD.01.01.00 10-0008/18. We gratefully acknowledge Polish high-performance computing infrastructure PLGrid (HPC Centers: ACK Cyfronet AGH) for providing computer facilities and support within computational grant no PLG/2025/018737. Funding obtained from the Czech Science Foundation through the joint GAČR–NCN project 24-15057L is gratefully acknowledged. The computational resources were provided by the e-INFRA CZ project (ID:90254) and by the ELIXIR-CZ project (ID:90255), which are part of the international ELIXIR infrastructure. Authors are grateful to Dr Bak-Sypien for technical support.

References

1 P. H. Schafer, F. Truzzi, A. Parton, L. Wu, J. Kosek, L.-H. Zhang, G. Horan, A. Saltari, M. Quadri, R. Lotti, A. Marconi and C. Pincelli, *Cell. Signal.*, 2016, **28**, 753–763.
2 G. M. Keating, *Drugs*, 2017, **77**, 459–472.
3 A. Gottlieb, N. J. Korman, K. B. Gordon, S. R. Feldman, M. Lebwohl, J. Y. M. Koo, A. S. Van Voorhees, C. A. Elmets, C. L. Leonardi, K. R. Beutner, R. Bhushan and A. Menter, *J. Am. Acad. Dermatol.*, 2008, **58**, 851–864.
4 A. Menter, A. Gottlieb, S. R. Feldman, A. S. Van Voorhees, C. L. Leonardi, K. B. Gordon, M. Lebwohl, J. Y. M. Koo, C. A. Elmets, N. J. Korman, K. R. Beutner and R. Bhushan, *J. Am. Acad. Dermatol.*, 2008, **58**, 826–850.
5 M. G. Lebwohl, H. Bachelez, J. Barker, G. Girolomoni, A. Kavanaugh, R. G. Langley, C. F. Paul, L. Puig, K. Reich and P. C. M. Van De Kerkhof, *J. Am. Acad. Dermatol.*, 2014, **70**, 871–881.
6 G. Goldenberg, J. Lanoue and J. Dong, *J. Clin. Aesthet. Dermatol.*, 2016, **9**, 25–28.
7 https://www.who.int/publications/i/item/9789241565189, Global report on psoriasis.
8 Press Announcements > FDA approves Otezla to treat psoriatic arthritis.
9 Apremilast for the Treatment of Psoriatic Arthritis, American College of Rheumatology, ACRA.
10 D. P. Agrawal, D. V. Kushwaha, D. S. Siddiqui, D. S. R. Singh and D. G. S. Rana, *Int. J. Pharm. Sci. Rev. Res.*, 2025, 98–104.
11 A. Ainurofiq, D. Putro, D. Ramadhani, G. Putra and L. C. Do Espirito Santo, *J. Rep. Pharm. Sci.*, 2021, **10**, 137.
12 A. Bhakay, M. Rahman, R. N. Dave and E. Bilgili, *Pharmaceutics*, 2018, **10**, 86.
13 N. Blagden, M. De Matas, P. T. Gavan and P. York, *Adv. Drug Deliv. Rev.*, 2007, **59**, 617–630.
14 M. Singh, M. P. Sawarkar, M. R. Dhondale, D. R. Serrano, A. K. Agrawal and D. Kumar, *Cryst. Growth Des.*, 2025, **25**, 7852–7868.
15 J. Pantwalawalkar, N. Kale, S. Nangare, S. Patil, S. Pawar and N. Jadhav, *J. Drug Deliv. Sci. Technol.*, 2025, **104**, 106572.
16 N. K. Duggirala, M. L. Perry, Ö. Almarsson and M. J. Zaworotko, *Chem. Commun.*, 2016, **52**, 640–655.
17 J. Jirát, M. Babor, L. Ridvan, E. Skořepová, M. Dušek and M. Šoóš, *IUCrJ*, 2022, **9**, 508–515.
18 F.-Y. Wang, Q. Zhang, Z. Zhang, X. Gong, J.-R. Wang and X. Mei, *CrystEngComm*, 2018, **20**, 5945–5948.
19 Y. Naumkina, B. Kratochvíl, E. Korotkova and J. Čejka, *Molecules*, 2024, **29**, 6060.
20 M. K. Dudek, M. Kostrzewa, P. Paluch and M. J. Potrzebowski, *Cryst. Growth Des.*, 2018, **18**, 3959–3970.
21 M. K. Dudek, E. Wielgus, P. Paluch, J. Śniechowska, M. Kostrzewa, G. M. Day, G. D. Bujacz and M. J. Potrzebowski, *Acta Crystallogr. Sect. B:Struct. Sci.*, 2019, **75**, 803–814.
22 J. Jirát, D. Ondo, M. Babor, L. Ridvan and M. Šoóš, *Int. J. Pharm.*, 2019, **570**, 118639.
23 D. Douroumis, S. A. Ross and A. Nokhodchi, *Adv. Drug Deliv. Rev.*, 2017, **117**, 178–195.
24 S. L. James, C. J. Adams, C. Bolm, D. Braga, P. Collier, T. Friščić, F. Grepioni, K. D. M. Harris, G. Hyett, W. Jones, A. Krebs, J. Mack, L. Maini, A. G. Orpen, I. P. Parkin, W. C. Shearouse, J. W. Steed and D. C. Waddell, *Chem. Soc. Rev.*, 2012, **41**, 413–447.
25 M. Solares-Briones, G. Coyote-Dotor, J. C. Páez-Franco, M. R. Zermeño-Ortega, C. M. De La O Contreras, D. Canseco-González, A. Avila-Sorrosa, D. Morales-Morales and J. M. Germán-Acacio, *Pharmaceutics*, 2021, **13**, 790.
26 R. Thipparaboina, D. Kumar, R. B. Chavan and N. R. Shastri, *Drug Discov. Today*, 2016, **21**, 481–490.
27 I. D'Abbrunzo, E. Bianco, L. Gigli, N. Demitri, R. Birolo, M. R. Chierotti, I. Škorić, J. Keiser, C. Häberli, D. Voinovich, D. Hasa and B. Perissutti, *Int. J. Pharm.*, 2023, **644**, 123315.
28 I. D'Abbrunzo, E. Venier, F. Selmin, I. Škorić, E. Bernardo, G. Procida and B. Perissutti, *Pharmaceutics*, 2025, **17**, 92.
29 A. Port, C. Almansa, R. Enrech, M. Bordas and C. R. Plata-Salamán, *Cryst. Growth Des.*, 2019, **19**, 3172–3182.
30 R. Thakuria and B. Sarma, *Crystals*, 2018, **8**, 101.
31 G. A. Bowmaker, *Chem. Commun.*, 2013, **49**, 334–348.

32 S. Grabowski, J. Wojdyła-Parat, M. Tyszka-Czochara, M. Kozieł, M. Chmylak, S. Lalik and M. Gryl, *Chem. Commun.*, 2025, **61**, 16770–16773.
33 G. M. Sheldrick, *Acta Crystallogr., Sect. A*, 2015, **71**, 3–8.
34 O. V. Dolomanov, L. J. Bourhis, R. J. Gildea, J. A. K. Howard and H. Puschmann, *J. Appl. Crystallogr.*, 2009, **42**, 339–341.
35 S. J. Clark, M. D. Segall, C. J. Pickard, P. J. Hasnip, M. I. J. Probert, K. Refson and M. C. Payne, *Z. Kristallogr. Cryst. Mater.*, 2005, **220**, 567–570.
36 A. Tkatchenko and M. Scheffler, *Phys. Rev. Lett.*, 2009, **102**, 073005.
37 L. Kronik and A. Tkatchenko, *Acc. Chem. Res.*, 2014, **47**, 3208–3216.
38 W. P. Wood, M. Arhangelskis, E. Bartůňková, C. E. S. Bernardes, A. D. Boese, D. E. Braun, D.-K. Bučar, H. Butkiewicz, C. Červinka, B. Civalleri, N. Couvrat, E. De Ronde, L. Donà, M. Dračínský, D. Firaha, M. Fulem, R. Geronia Ii, N. Goncharova, M. Gryl, J. Hoja, A. Hoser, J. Krzeszczakowska, A. List, I. Lončarić, B. Mladineo, J. Nyman, E. Olehovics, M. Raimondo, I. B. Rietveld, R. I. S. Rodrigues, L. Russo, M. Salvalaglio, M. Sarraguça, J. Šnajdr, V. Štejfa, G. Sun, P. Tinnemans, P. S. Whitfield, Z. Yang, Y. Zhang and S. L. Price, *Cryst. Growth Des.*, 2026, **26**, 476–493.
39 A. D. Becke, *J. Chem. Phys.*, 1993, **98**, 5648–5652.
40 G. Kresse and D. Joubert, *Phys. Rev. B*, 1999, **59**, 1758–1775.
41 M. D. Segall, P. J. D. Lindan, M. J. Probert, C. J. Pickard, P. J. Hasnip, S. J. Clark and M. C. Payne, *J. Phys.: Condens. Matter*, 2002, **14**, 2717–2744.
42 J. Rohlíček, V. Eigner, J. Czernek and J. Brus, *J. Appl. Crystallogr.*, 2025, **58**, 321–332.
43 M. J. Frisch, G. W. Trucks, H. B. Schlegel, G. E. Scuseria, M. A. Robb, J. R. Cheeseman, G. Scalmani, V. Barone, G. A. Petersson, H. Nakatsuji, X. Li, M. Caricato, A. V. Marenich, J. Bloino, B. G. Janesko, R. Gomperts, B. Mennucci, H. P. Hratchian, J. V. Ortiz, A. F. Izmaylov, J. L. Sonnenberg, D. Williams-Young, F. Ding, F. Lipparini, F. Egidi, J. Goings, B. Peng, A. Petrone, T. Henderson, D. Ranasinghe, V. G. Zakrzewski, J. Gao, N. Rega, G. Zheng, W. Liang, M. Hada, M. Ehara, K. Toyota, R. Fukuda, J. Hasegawa, M. Ishida, T. Nakajima, Y. Honda, O. Kitao, H. Nakai, T. Vreven, K. Throssell, J. A. Montgomery, Jr., J. E. Peralta, F. Ogliaro, M. J. Bearpark, J. J. Heyd, E. N. Brothers, K. N. Kudin, V. N. Staroverov, T. A. Keith, R. Kobayashi, J. Normand, K. Raghavachari, A. P. Rendell, J. C. Burant, S. S. Iyengar, J. Tomasi, M. Cossi, J. M. Millam, M. Klene, C. Adamo, R. Cammi, J. W. Ochterski, R. L. Martin, K. Morokuma, O. Farkas, J. B. Foresman, and D. J. Fox, *Gaussian 16, Revision B.01 (Version GaussView 5.0.)*, Gaussian Inc. Wallingford CT, 2016.
44 J. Czernek and J. Brus, *Int. J. Mol. Sci.*, 2020, **21**, 7908.
45 M. Oracz, P. Garczarek, P. Skoczen, D. Podwysocka, M. Szulc and A. Majewski, Crystalline Forms of Apremilast, International Patent Application, WO2017/196192A1, 2017.
46 Q. Zhang, Y. Yan, A. Li, Y. Xu and X. Zhang, *Cryst. Growth Des.*, 2025, **25**, 6558–6565.
47 J. Jirát, V. Zvoníček, M. Babor, L. Ridvan, E. Skořepová, M. Dušek and M. Šoóš, *Cryst. Growth Des.*, 2020, **20**, 5785–5795.
48 M. K. Dudek, K. Trzeciak, L. Tajber, J. Zając, S. Kaźmierski, E. Pindelska, T. Makowski, M. Svyntkivska and M. J. Potrzebowski, *Chem.–Eur. J.*, 2024, **30**, e202302138.
49 K. Trzeciak, M. K. Dudek and M. J. Potrzebowski, *Chem.–Eur. J.*, 2024, **30**, e202402683.
50 A. V. Trask, W. D. S. Motherwell and W. Jones, *Chem. Commun.*, 2004, 890–891.
51 T. Friščić, S. L. Childs, S. A. A. Rizvi and W. Jones, *CrystEngComm*, 2009, **11**, 418–426.
52 S. Aitipamula, P. S. Chow and R. B. H. Tan, *CrystEngComm*, 2009, **11**, 1823–1827.
53 M. Przybyłek, D. Ziółkowska, K. Mroczyńska and P. Cysewski, *Eur. J. Pharm. Sci.*, 2016, **85**, 132–140.
54 A. Sokal, E. Pindelska, L. Szeleszczuk and W. Kolodziejski, *Int. J. Pharm.*, 2017, **522**, 80–89.
55 V. M. Hariprasad, S. K. Nechipadappu and D. R. Trivedi, *Cryst. Growth Des.*, 2016, **16**, 4473–4481.
56 E. Muñoz-Hernández, C. Alarcón-Payer, A. Frontera, R. Prohens, R. Barbas, F. J. Acebedo-Martínez, A. Domínguez-Martín and D. Choquesillo-Lazarte, *CrystEngComm*, 2026, **28**, 88–100.
57 S. Pagola and P. W. Stephens, *Acta Crystallogr., Sect. C: Struct. Chem.*, 2009, **65**, o583–o586.
58 D. A. Druzhbin, T. N. Drebushchak, V. S. Min'kov and E. V. Boldyreva, *J. Struct. Chem.*, 2015, **56**, 317–323.
59 M.-A. Perrin, M. A. Neumann, H. Elmaleh and L. Zaske, *Chem. Commun.*, 2009, **3181**.
60 J. C. Burley, M. J. Duer, R. S. Stein and R. M. Vrcelj, *Eur. J. Pharm. Sci.*, 2007, **31**, 271–276.
61 E. Pardhi, D. S. Tomar, R. Khemchandani, G. Samanthula, P. K. Singh and N. K. Mehra, *J. Mol. Struct.*, 2024, **1299**, 137045.
62 R. Khemchandani, E. Pardhi, A. Jadhav, P. Devi, K. Roshitha, N. Bhatt, C. Godugu, N. K. Mehra and G. Samanthula, *Int. J. Pharm.*, 2025, **686**, 126283.
63 A. D. Becke, *J. Chem. Phys.*, 1993, **98**, 5648–5652.
64 Y. Naumkina, B. Kratochvíl, E. Korotkova and J. Čejka, *CrystEngComm*, 2025, **27**, 7713–7720.
65 S. J. Dengale, H. Grohganz, T. Rades and K. Löbmann, *Adv. Drug Deliv. Rev.*, 2016, **100**, 116–125.
66 C. R. Taylor and G. M. Day, *Cryst. Growth Des.*, 2018, **18**, 892–904.
67 M. Boncler, M. Lukasiak, J. Dastych, J. Golanski and C. Watala, *Basic Clin. Pharmacol. Toxicol.*, 2019, **124**, 199–210.
68 CCDC 2513155: Experimental Crystal Structure Determination, 2026, DOI: 10.5517/ccdc.csd.cc2qc4js.